© 2016. Published by The Company of Biologists Ltd | Journal of Cell Science (2016) 129, 983-993 doi:10.1242/jcs.175802

RESEARCH ARTICLE

Unique and redundant β-catenin regulatory roles of two Dishevelled paralogs during *C. elegans* asymmetric cell division

Austin T. Baldwin, Amy M. Clemons and Bryan T. Phillips*

ABSTRACT

The Wnt/β-catenin signaling pathway is utilized across metazoans. However, the mechanism of signal transduction, especially dissociation of the β-catenin destruction complex by Dishevelled proteins, remains controversial. Here, we describe the function of the Dishevelled paralogs DSH-2 and MIG-5 in the Wnt/β-catenin asymmetry (WβA) pathway in *Caenorhabditis elegans*, where WβA drives asymmetric cell divisions throughout development. We find that DSH-2 and MIG-5 redundantly regulate cell fate in hypodermal seam cells. Similarly, both DSH-2 and MIG-5 are required for positive regulation of SYS-1 (a *C. elegans* β-catenin), but MIG-5 has a stronger effect on the polarity of SYS-1 localization. We show that MIG-5 controls cortical APR-1 (the *C. elegans* APC) localization. DSH-2 and MIG-5 both regulate the localization of WRM-1 (another *C. elegans* β-catenin), acting together as negative regulators of WRM-1 nuclear localization. Finally, we demonstrate that overexpression of DSH-2 or MIG-5 in seam cells leads to stabilization of SYS-1 in the anterior seam daughter, solidifying the Dishevelled proteins as positive regulators of SYS-1. Overall, we have further defined the role of Dishevelled in the WβA signaling pathway, and demonstrated that DSH-2 and MIG-5 regulate cell fate, β-catenin nuclear levels and the polarity of β-catenin regulation.

KEY WORDS: APC, Asymmetric Cell Division, β-Catenin, Dishevelled, Wnt

INTRODUCTION

Multicellular organisms use a variety of mechanisms and strategies to control gene activation in developmental and homeostatic processes. One widely used scheme is the Wnt/β-catenin signaling pathway, which controls the stability of the transcriptional activator β-catenin and its interaction with the transcription factor TCF. Wnt/β-catenin signaling in mammals is used to control processes as diverse as axial specification, heart development and adult stem cell proliferation (Clevers and Nusse, 2012; Gessert and Kühl, 2010; Hikasa and Sokol, 2013; Houston, 2012; McMahon and Moon, 1989). Although many core and auxiliary proteins involved in Wnt/β-catenin signaling have been identified, the mechanism and significance of the interactions involved in key steps of the Wnt signal cascade are lacking. Additionally, although the identities of the major players of Wnt/β-catenin signaling are widely accepted, how those players interact *in vivo* to transduce the Wnt signal remains a major unresolved question among and within various tissues and organisms.

Department of Biology, University of Iowa, 143 Biology Building, Iowa City, IA 52242-1324, USA.

*Author for correspondence (bryan-phillips@uiowa.edu)

Received 12 June 2015; Accepted 13 January 2016

Our current understanding of Wnt/β-catenin signaling is that in the absence of the extracellular Wnt signal, cytoplasmic β-catenin is bound, phosphorylated and ubiquitylated by a group of proteins known as the 'destruction complex' (Clevers and Nusse, 2012). The canonical destruction complex includes the scaffold proteins APC and Axin and the kinases casein kinase 1α (CKIα, also known as CSNK1A1) and glycogen synthase kinase 3β (GSK3β). TCF proteins bind to regulatory regions of target genes, but in the absence of nuclear β-catenin interact with corepressors and downregulate gene expression (Roose et al., 1998). When a Frizzled (Fz) receptor is bound by the extracellular Wnt ligand, a signaling cascade commences that results in the inactivation of the destruction complex and stabilization of cytoplasmic β-catenin. Increased cytoplasmic levels of β-catenin result in higher nuclear levels of β-catenin, and the interaction between β-catenin and TCF in the nucleus results in the activation of Wnt target genes. Mutations of β-catenin and/or destruction complex members that result in inappropriate β-catenin stabilization lead to constitutive activation of Wnt target genes; in stem cell populations, such as those of the human intestinal lining or breast, constitutive activation of Wnt targets can result in tumor formation and proliferation (Barker et al., 2009; Groden et al., 1991; Khramtsov et al., 2010; Webster et al., 2000). Thus, understanding the mechanisms that control Wnt/β-catenin signal transduction and destruction complex activation have great implications for human health in addition to informing our knowledge of development and stem cell biology.

In *Caenorhabditis elegans*, most asymmetric cell divisions (ACDs) are controlled by a Wnt pathway that uses β-catenin–TCF interactions to differentially control transcription of target genes in the two daughter cells after ACD. This Wnt/β-catenin asymmetry (WβA) signaling pathway can be most simply described as an adaptation of the canonical Wnt/β-catenin signaling pathway within the context of an asymmetric cell division; a mother cell that has polarized localization of conserved Wnt signaling components divides to produce daughter cells with asymmetric inheritance of Wnt signaling components, which ultimately translates to asymmetric activation of Wnt target genes (Sawa, 2012). The pathway contains two branches: one that more closely resembles the canonical pathway, which controls the stability of SYS-1 (one of the *C. elegans* β-catenins), and another non-canonical pathway where the nuclear localization of POP-1 (a *C. elegans* TCF) is regulated by another β-catenin, WRM-1 (Fig. S1) (Phillips and Kimble, 2009). The result is that the anterior daughter nucleus contains low levels of SYS-1 and WRM-1 leading to target gene repression, whereas the posterior daughter nucleus contains high levels of SYS-1 and WRM-1, leading to target gene activation.

Despite some clear mechanistic departures from canonical Wnt/β-catenin signaling, specifically the regulation of nuclear TCF, WβA holds much in common with the canonical pathway. Asymmetric SYS-1 levels are controlled by the conserved destruction complex members APR-1, PRY-1 and KIN-19 (the *Caenorhabditis elegans*

Journal of Cell Science (2016) 129, 983-993 doi:10.1242/jcs.175802

APC, Axin and CKIα, respectively), and the proteasome, indicating that its stability is likely to be regulated similarly to canonical β-catenin, but adapted for ACD (Baldwin and Phillips, 2014; Huang et al., 2007; Phillips et al., 2007; Vora and Phillips, 2015). WRM-1 localization is also controlled by APR-1, PRY-1 and KIN-19, with the difference being that nuclear WRM-1 levels are controlled by protein trafficking. This trafficking is rendered asymmetric by the asymmetric localization of APR-1, which stabilizes microtubules in a conserved fashion (a summary of prior models of WβA signaling can be found in Fig. S1) (Baldwin and Phillips, 2014; Mizumoto and Sawa, 2007; Rocheleau et al., 1999; Sugioka and Sawa, 2012; Takeshita and Sawa, 2005). Finally, both pathways have similar unanswered questions surrounding the transduction of the Wnt signal: in both pathways it is clear that cells are responding to extracellular Wnt cues and transducing those cues into inactivation of the β-catenin destruction complex, but how this transduction occurs remains unresolved in both pathways.

In the canonical Wnt/β-catenin pathway, activation of Wnt signaling results in the Dishevelled (Dvl) scaffold protein binding to a Fz receptor (Wong et al., 2003). Dvl then binds and sequesters Axin, inactivating β-catenin degradation (Cliffe et al., 2003; Fiedler et al., 2011; Itoh et al., 2000). How exactly the destruction complex is inactivated remains controversial, with several models proposing inactivation of β-catenin phosphorylation mediating destruction complex inactivation or dissociation, whereas a recent model proposes that the complex remains intact, although inactivated, during signal transduction (Lee et al., 2003; Li et al., 2012; Mao et al., 2001; Taelman et al., 2010). In the hypodermal seam cells of *C. elegans*, several Wnt ligands and receptors control the orientation of polarity of WβA activation (Yamamoto et al., 2011). Additionally, the *C. elegans* Dvl paralogs DSH-2 and MIG-5 have been shown to be involved in WβA signaling, but whether and how they polarize destruction complex inactivation is unclear (Chang et al., 2005; King et al., 2009; Phillips et al., 2007; Sugioka et al., 2011). Thus, given the similar unresolved questions in both canonical and WβA signaling, investigating the role of Dvl in signal transduction in WβA might also provide insights into canonical Wnt/β-catenin signaling activation.

Previously, we have demonstrated that WβA signaling appears to subdivide APR-1 into two functional pools during asymmetric cell division: one pool that regulates SYS-1 localization and one pool that regulates WRM-1 localization (Baldwin and Phillips, 2014). Here, we show that the Dvl proteins DSH-2 and MIG-5 redundantly control cell fate specification during ACD. Additionally, we show that DSH-2 and MIG-5 are both necessary to properly regulate SYS-1 and WRM-1 localization, but that their functions in regulating SYS-1, WRM-1 and APR-1 localization are each specialized. We also demonstrate that neither DSH-2 nor MIG-5 control PRY-1 localization, suggesting that the ultimate target of Dvl regulation in WβA is APR-1. Finally, we show that overexpression of MIG-5 and DSH-2 results in recruitment of SYS-1 into Dvl-containing puncta and SYS-1 stabilization in anterior (unsignaled) daughter cells. In total, we show that DSH-2 and MIG-5 have both redundant and non-redundant roles in the control of β-catenin localization in *C. elegans* ACDs. This result demonstrates that Dvl paralogs can cooperate to fulfill conserved roles in Wnt/β-catenin signaling while also having individualized functions, providing insight into roles multiple Dvl proteins can have in the Wnt signal cascade.

RESULTS

DSH-2 and MIG-5 control seam cell fate

WβA signaling has been shown to control cell fate in the asymmetric cell divisions of the *C. elegans* hypodermal seam cells (Banerjee et al., 2010; Gleason and Eisenmann, 2010; Gorrepati et al., 2013; Hughes et al., 2013; Ren and Zhang, 2010; Yamamoto et al., 2011). The *C. elegans* seam is composed of two lines of hypodermal cells, one each on the left and right sides of the worm. The seam cells are essential for expression of various collagens that assemble the outer cuticle of the worm (Liu et al., 1995; Thein et al., 2003) and also generate the cuticle alae structure during L1 and adult stages (Costa et al., 1997; Singh and Sulston, 1978). Over the course of larval development the seam cells divide several times, generally in an asymmetric pattern that produces an anterior daughter that fuses to the hypodermal syncytium hyp7, and a posterior daughter that retains the seam fate and positioning (Sulston and Horvitz, 1977). This 'stem-cell-like' mode of division allows the seam cells to repeatedly contribute additional nuclei to the growing hyp7 syncytium while maintaining a consistent seam cell number and structure (Fig. S2).

In order to determine the roles of DSH-2 and MIG-5 in WβA signaling, we investigated the function of each gene in determining seam cell fate. Although WβA controls many asymmetric divisions in *C. elegans*, the divisions of the seam cells are easily observable and study of their divisions might provide insights into stem cell biology as well as Wnt/β-catenin signaling. Previous experiments using RNA interference (RNAi) have shown that depletion of *dsh-2* or *mig-5* does not have any effect on seam cell number (Banerjee et al., 2010). Thus, we utilized the deletion mutants *dsh-2(or302)* and *mig-5(tm2639)*, hereafter referred to as *dsh-2* and *mig-5*, respectively. Both mutations are sizeable insertions or deletions that also result in frameshifts, likely causing complete loss-of-function (Hawkins et al., 2005). When crossed with *wIs51* [expressing GFP under a seam cell promoter (P_{scm}::GFP)], both *dsh-2* and *mig-5* resulted in statistically significant alterations in seam cell number ($P<0.01$, *t*-test; Fig. 1). Interestingly, both mutants displayed both gains and losses of seam cells when compared to wild type. Gains of seam cells are associated with loss of function in negative regulators of Wnt signaling, such as APR-1 or KIN-19 (Banerjee et al., 2010; Gleason and Eisenmann, 2010; Ren and Zhang, 2010). Conversely, losses of seam cells are associated with loss of function of positive regulators of Wnt target gene activation, such as WRM-1 or LIT-1. Treatments that result in both gains and losses might represent disruption of the machinery that polarizes the WβA function (Yamamoto et al., 2011), resulting in randomized ACD or symmetric division. Thus, as *dsh-2* and *mig-5* result in both gains and losses of seam cells, they are likely involved in polarizing the seam cell fate decision. However, the *dsh-2 mig-5* double mutant displays a significant increase in seam cell number compared to either single mutant and appears to abrogate most losses of seam cells, indicating that in sum the two Dvl paralogs function together as negative regulators of seam cell fate (Fig. 1C, see also Fig. 6 and the Discussion for further interpretation).

A third *C. elegans* homolog of Dvl, DSH-1, has not been directly implicated in WβA signaling. Previous work has shown that knockdown of DSH-1 results in wild-type numbers of seam cells, although mild suppression of seam cell hyperplasia has been observed in a *dsh-1*, *kin-19* double RNAi experiment (Banerjee et al., 2010). To more definitively resolve a role for DSH-1 in seam cell specification, we quantified seam cell numbers using the *dsh-1* deletion allele (*ok1445*) (Table S1). We did not find any significant changes in seam cell number in *dsh-1(ok1445)* compared to wild-type worms (Table S1). However, it remained possible that DSH-1 function in the seam cells could be redundant with DSH-2 and MIG-5, so we combined *dsh-1(RNAi)* with the *dsh-2 mig-5* double mutant. The *dsh-2 mig-5*, *dsh-1(RNAi)* treatment did not

Journal of Cell Science (2016) 129, 983-993 doi:10.1242/jcs.175802

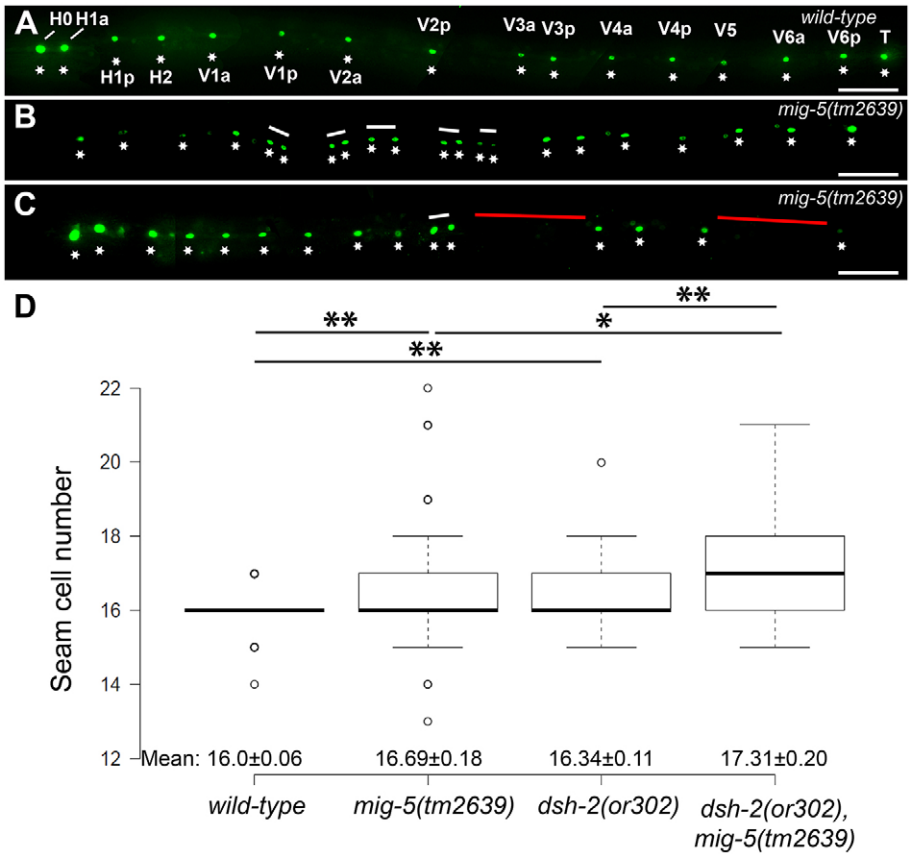

Fig. 1. DSH-2 and MIG-5 redundantly control seam cell fate specification. (A) Representative image of a wild-type worm expressing *wIs51*(P_{scm}::GFP) in 16 seam cells (seam cell nuclei marked with asterisks). The L1-stage progenitors of each seam cell are also labeled. (B) Representative image of *mig-5(tm2639)* worm expressing *wIs51* in 21 seam cells. (C) Representative image of a *mig-5 (tm2639)* worm expressing *wIs51* in seam cells. Presumed gains and losses of seam cells as a result of aberrant symmetric division are denoted with white and red bars, respectively. Scale bars: 50 µm. In order to image the complete length of the worms in A–C, multiple images of the same worm were acquired, and composite images are shown. (D) Box plot showing seam cell count for each listed genotype. Center lines show the medians; box limits indicate the 25th and 75th percentiles as determined by R software; whiskers extend for 1.5 times the interquartile range from the 25th and 75th percentiles, outliers are represented by dots. **P*<0.05, ***P*<0.01 (*t*-test). The mean±s.e.m. is displayed below the box plot. *n*=66 (wild type), 72 (*mig-5*), 63 (*dsh-2*) and 58 (*dsh-2*, *mig-5*).

result in any changes in seam cell number compared to *dsh-2 mig-5* (Table S1). We thus conclude that DSH-1 is not a major contributor to asymmetric cell division of the seam cells, and we focused the remainder of our experiments on DSH-2 and MIG-5.

DSH-2 and MIG-5 both control SYS-1 localization, but only MIG-5 controls APR-1 localization

Having established that DSH-2 and MIG-5 control seam cell fate, we investigated whether *dsh-2* and *mig-5* mutants display disruption in the localization of WβA components. In canonical Wnt/β-catenin signaling, Dvl acts downstream of Wnt ligands and Fz receptors and upstream of the β-catenin destruction complex (Clevers and Nusse, 2012). Given that Dvl proteins responds to upstream signals in multiple ways to function in multiple Wnt pathways (Dillman et al., 2013; Gao and Chen, 2010), we focused on the DSH-2- and MIG-5-mediated regulation of downstream Wnt components to determine how they regulate the complex outputs of WβA signaling. Thus, we crossed the *uiwIs4*(P_{sys-1}::mCherry::SYS-1) transgene into *dsh-2*, *mig-5*, and *dsh-2 mig-5* mutants and observed the localization of both transgenes during the terminal seam cell division as we described previously (Baldwin and Phillips, 2014). In this final division during wild-type development, mCh::SYS-1 localizes asymmetrically to seam cell daughter nuclei (Fig. 2A) (Baldwin and Phillips, 2014). In *mig-5* mutant worms, we found that average nuclear mCh::SYS-1 fluorescence was significantly reduced in both anterior and posterior daughters compared to wild type. This reduction resulted in daughter cells where anterior and posterior mCh::SYS-1 fluorescence levels were no longer significantly different from each other (*P*=0.067) (Fig. 2B,E). In *dsh-2* mutant worms, average mCh::SYS-1 fluorescence was also significantly reduced in both anterior and posterior daughters compared to wild type, but anterior and posterior mCh::SYS-1 fluorescence levels remained significantly different from each other (*P*<0.001) (Fig. 2C,E). Given that both single mutants caused reductions of SYS-1 levels, we examined *dsh-2 mig-5* double mutants to determine whether the Dvl paralogs had redundant functions. In the *dsh-2 mig-5* double mutant, average nuclear mCh::SYS-1 fluorescence in both daughters was significantly reduced compared to wild type (Fig. 2E). Additionally, the *dsh-2 mig-5* double mutant posterior daughter displayed significantly reduced SYS-1 compared to posterior daughters of *dsh-2* single mutants (Fig. 2E). No significant difference was observed between anterior and posterior mCh::SYS-1 in *dsh-2 mig-5* double mutants (*P*=0.653) (Fig. 2E), indicating that these divisions had been rendered symmetric. Given the reduction of nuclear mCh::SYS-1 in *dsh-2* and *mig-5* single and double mutants, we conclude that DSH-2 and MIG-5 act as positive regulators of nuclear SYS-1. Additionally, as the *dsh-2 mig-5* mutant phenotype significantly differs from *dsh-2* but not *mig-5* mutants, it is possible that the unique MIG-5 function is genetically downstream of DSH-2 in SYS-1 regulation.

As APR-1 is a known negative regulator of SYS-1 and likely to be downstream of Dvl function in WβA, we crossed both *osIs13* (P_{apr-1}::APR-1::YFP) and *uiwIs4* (mCh::SYS-1) into *dsh-2* and *mig-5* mutants in order to observe whether changes in SYS-1 localization were accompanied by changes in APR-1 localization (Baldwin and Phillips, 2014). As we and others have previously demonstrated, APR-1::YFP localizes to the anterior seam cell cortex, whereas mCh::SYS-1 localizes asymmetrically to daughter cell nuclei (Fig. 2F) (Baldwin and Phillips, 2014; Mizumoto and Sawa, 2007; Wildwater et al., 2011). In *mig-5* mutants, levels of cortical APR-1::VNS appear elevated in the posterior daughter when compared to wild type, indicating that MIG-5 is required for

Journal of Cell Science (2016) 129, 983-993 doi:10.1242/jcs.175802

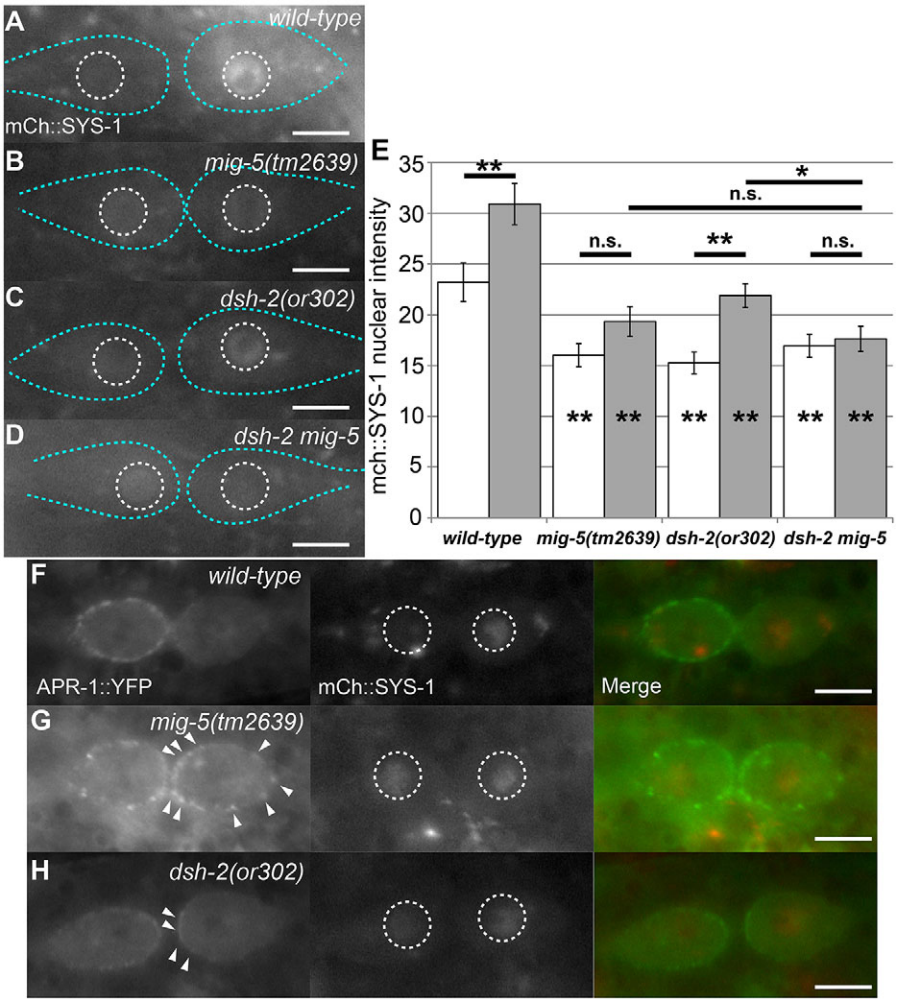

Fig. 2. DSH-2 and MIG-5 both regulate SYS-1 localization, but only MIG-5 regulates cortical APR-1 localization. (A–D) Representative images of seam cell daughters expressing *uiwIs4*(P_{sys-1}::mCherry::SYS-1/β-catenin). A, wild type; B, *mig-5(tm2639)*; C, *dsh-2(or302)*; D, *dsh-2(or302) mig-5(tm2639)*. (E) Mean±s.e.m. mCherry::SYS-1 nuclear intensity for each listed genotype. *n*=33 for all genotypes. (F–H) Representative images of seam cell daughters expressing *osIs13*(P_{apr-1}::APR-1/APC::YFP) (left column) and *uiwIs4*(P_{sys-1}::mCherry::SYS-1/β-catenin) (middle column), and the merge *osIs13+uiwIs4* (right column). F, wild type; G, *mig-5(tm2639)*; H, *dsh-2(or302)*. In A–D, blue dashed lines represent cell boundaries, and dashed circles represent nuclei. In E and I, white columns indicate anterior nucleus fluorescence; gray columns indicate posterior nucleus fluorescence. Asterisks inside columns indicate statistical comparison to corresponding wild-type column. Horizontal lines represent the statistical comparisons indicated. ***P*<0.01; n.s., *P*>0.05 (Mann–Whitney test). In F–H, arrowheads indicate cortical APR-1::YFP puncta, and dashed circles indicate nuclei. Scale bars: 5 µm.

cortical polarization of APR-1 (Fig. 2G). Conversely, cortical APR-1 localization is largely unperturbed in *dsh-2* mutants, although occasional posterior puncta were observed (Fig. 2H, arrowheads). To better describe changes in APR-1 localization, we scored divisions on whether cortical levels appeared to be higher in the anterior daughter, the posterior daughter or neither (Table 1). *mig-5* mutants displayed a significantly altered distribution of APR-1::YFP compared to wild type ($P<0.001$, Fisher's exact test), whereas APR-1 distribution in *dsh-2* mutants was not significantly perturbed ($P=0.057$, Fisher's exact test). We also note that SYS-1 fluorescence was significantly higher in *dsh-2* and *mig-5* mutants expressing APR-1::YFP than in those that did not express APR-1::YFP (Fig. 2G,H), although this is likely an artifact of APR-1 overexpression in a Dvl mutant background. A *dsh-2 mig-5* double mutant expressing APR-1::YFP was also constructed, but homozygotes died as embryos or arrested as L1 larvae, preventing observation of the final seam cell division (data not shown). Thus, mutation of *mig-5* results in clear APR-1 polarity defects, whereas mutation of *dsh-2* does not, agreeing with the defects in SYS-1 nuclear asymmetry observed for each mutant.

Table 1. Cortical APR-1::YFP distribution

	Cortical APR-1::YFP distribution			
	A>P	A=P	A<P	Total
Wild type	52	1	1	54
mig-5(tm2639)	12	17	0	29
dsh-2(or302)	23	4	1	28

A indicates anterior, P indicates posterior.

DSH-2 and MIG-5 have distinct functions in WRM-1 regulation

Given that MIG-5 controls APR-1 localization and APR-1 controls both β-catenin outputs in the WβA pathway, we visualized WRM-1::GFP to functionally analyze the WRM-1-regulating pool of APR-1 in seam cell divisions lacking Dvl (Baldwin and Phillips, 2014; Mizumoto and Sawa, 2007). To do this, we combined both Dvl mutants with the *osIs5* (P_{scm}::WRM-1::YFP) transgene that we and others have previously reported to localize asymmetrically to seam cell daughter nuclei (Baldwin and Phillips, 2014; Hughes et al., 2013; Mizumoto and Sawa, 2007). *mig-5* mutants displayed a significant reduction in average nuclear WRM-1 levels in the posterior daughter nucleus, indicating that MIG-5 positively regulates WRM-1 levels in that daughter (Fig. 3B,E). This decrease in nuclear WRM-1 was accompanied by an increase in posterior cortical WRM-1, as would be expected from increased WRM-1 export (Mizumoto and Sawa, 2007; Sugioka et al., 2011). In *dsh-2* mutants, average WRM-1 levels in anterior and posterior nuclei are not significantly different from average WRM-1 levels in corresponding wild-type nuclei (Fig. 3E). However, although a statistically significant difference exists between anterior and posterior average nuclear WRM-1 levels in wild type (indicating

Journal of Cell Science (2016) 129, 983-993 doi:10.1242/jcs.175802

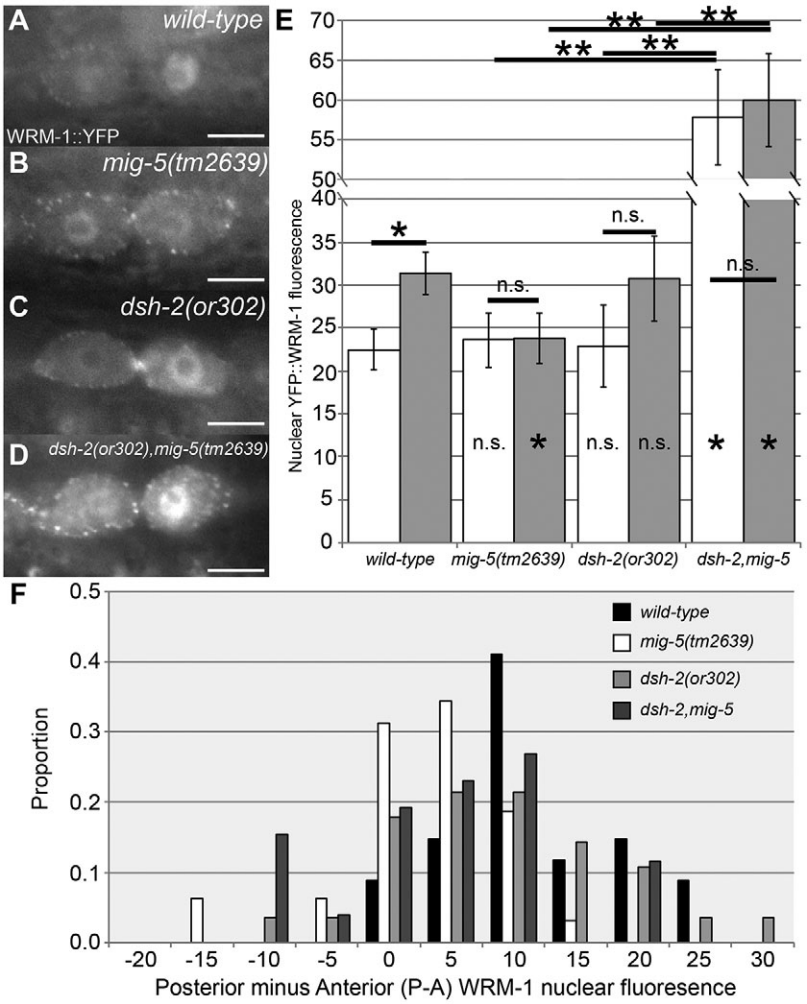

Fig. 3. DSH-2 and MIG-5 have different roles in WRM-1 regulation. (A–D) Representative images of *osIs5*(P_{scm}::WRM-1::YFP) localization in seam cell daughters. A, wild type; B, *mig-5(tm2639)*; C, *dsh-2(or302)*; D, *dsh-2(or302)*, *mig-5(tm2639)*. (E) Mean±s.e.m. WRM-1::YFP nuclear intensity. *n*=34 (wild type), 32 (*mig-5*), 25 (*dsh-2*), 26 (*dsh-2*,*mig-5*). White columns indicate anterior nucleus fluorescence; gray columns indicate posterior nucleus fluorescence. Asterisks inside columns indicate statistical comparison to corresponding wild-type column. Horizontal lines represent the statistical comparisons indicated. **P*<0.05; ***P*<0.01; n.s., *P*>0.05 (Mann–Whitney test). (F) 'Polarity index' of WRM-1::YFP nuclear intensity. Anterior intensity was subtracted from posterior intensity for each pair of daughter nuclei to estimate polarity of each division. Results are mean±s.e.m. Scale bars: 5 µm.

asymmetry), anterior and posterior average nuclear WRM-1 levels are not significantly different in *dsh-2* mutants (Fig. 3E). Thus some alteration to WRM-1 localization has likely occurred in *dsh-2* mutants despite the average WRM-1 nuclear levels being unaltered compared to wild type. This difference between the single mutants can be more clearly seen with a 'polarity index' calculated by subtracting anterior WRM-1 nuclear fluorescence from posterior in individual daughter pairs. In this analysis, *mig-5* mutants show a shift towards zero (i.e. symmetry) compared to wild type (Fig. 3F, white bars versus black bars). Conversely, *dsh-2* mutants follow a similar distribution to wild type but one that is slightly 'flatter', indicating that mutation of *dsh-2* might result in a very mild polarity defect for WRM-1 localization (Fig. 3F). From these data, MIG-5 has the most prominent role in controlling WRM-1 nuclear localization as seen from the significant decrease in posterior nuclear WRM-1 levels, which renders this division symmetric for nuclear WRM-1. Conversely, *dsh-2* appears to have little to no role in regulation of nuclear WRM-1 levels.

As the *mig-5* and *dsh-2* mutant phenotypes for WRM-1 were different, we observed WRM-1::YFP localization in the double mutant. Surprisingly, *dsh-2 mig-5* double mutants displayed average WRM-1 levels that were significantly higher in both anterior and posterior daughter nuclei when compared to wild-type, *mig-5* and *dsh-2* mutant seam cells (Fig. 3D,E). There was no statistically significant difference in WRM-1 fluorescence between the anterior and posterior nuclei in *dsh-2 mig-5* double mutants, indicating that loss of both DSH-2 and MIG-5 simultaneously results in WRM-1 polarity defects (Fig. 3E). When a 'polarity index' was constructed for *dsh-2 mig-5* double mutants, the distribution of asymmetry was broadened, similar to *dsh-2* mutants but it also had more reversals of polarity (Fig. 3F). The polarity index also demonstrates that although average WRM-1 levels were the same in anterior and posterior cells in *dsh-2 mig-5* mutants, many divisions still displayed a high degree of asymmetry, indicating that polarity of WRM-1 asymmetry is randomized (as can be seen in Fig. 3D). The *dsh-2 mig-5* double mutant distribution fails to strongly recapitulate either single mutant, which is consistent with individualized Dvl roles in the regulation of WRM-1 polarity, in addition to overlapping roles in regulation of WRM-1 nuclear levels. We conclude that DSH-2 and MIG-5 redundantly and negatively regulate nuclear levels of WRM-1, whereas MIG-5 is primarily responsible for regulating polarity of WRM-1 asymmetry.

PRY-1 localizes symmetrically to seam cell cortices

PRY-1 regulates APR-1 cortical localization (Baldwin and Phillips, 2014; Mizumoto and Sawa, 2007). As we have shown in Fig. 2 that *mig-5* disrupts cortical APR-1 asymmetry, we investigated whether either *mig-5* or *dsh-2* mutants could affect the localization of PRY-1. The functional PRY-1 construct *osEx229*(P_{pry-1}::PRY-1::GFP) has been previously reported to localize asymmetrically to the cortex of the earlier V5.p seam cell and its daughter cells (Fig. S2) (Mizumoto and Sawa, 2007). Observing the same construct at the

Journal of Cell Science (2016) 129, 983-993 doi:10.1242/jcs.175802

later terminal seam cell division, we found that PRY-1::GFP localized symmetrically to the cortex of both daughter cells in 90% of divisions (n=30) (Fig. 4A,B). Rare cases of apparent asymmetry were mild (see middle cell in Fig. 4A) and likely derived from focal plane changes given that the PRY-1 cortical domain is 'thin'. PRY-1::GFP cortical symmetry is likely biologically relevant because cells with lower levels of expression maintain symmetric PRY-1::GFP expression (Fig. S3A), and because PRY-1::GFP was not observed to induce fate changes in the seam cells, which were all observed to be differentiating asymmetrically (Fig. S3B, n=15). Despite lacking the hallmark asymmetry displayed by most WβA signaling components, we proceeded to determine whether MIG-5 and DSH-2 regulate PRY-1 localization. We found that PRY-1::GFP localized symmetrically to the cortex in 100% of *mig-5* mutant divisions (n=27), 93.4% of *dsh-2* mutant divisions (n=16), and 100% of *dsh-2 mig-5* divisions (n=15) (Fig. 4C–E). As we have previously demonstrated that *kin-19(RNAi)* disrupts APR-1 cortical asymmetry, we also examined whether KIN-19 controls PRY-1 cortical localization (Baldwin and Phillips, 2014). Again, we found that PRY-1::GFP localized symmetrically to seam daughter cortices in 90% of *kin-19(RNAi)* divisions (n=10) (Fig. 4F). Finally, we combined the Dvl mutants with *kin-19(RNAi)* to determine whether PRY-1::GFP localization could be disrupted in combination; however, PRY-1::GFP symmetrically localized to daughter cell cortices in all observed *mig-5; kin-19(RNAi)* and *dsh-2; kin-19(RNAi)* divisions (n=7 and 5, respectively) (Fig. 4G,H). From these experiments, we conclude that PRY-1 localizes symmetrically to the cortices of seam cell daughters and that MIG-5, DSH-2 and KIN-19 are unnecessary for this localization.

MIG-5 overexpression results in stabilization of SYS-1

Having uncovered the roles of DSH-2 and MIG-5 in controlling major downstream WβA signaling components, we turned to the localization of DSH-2 and MIG-5 themselves. Dvl localization is of special interest given the symmetric localization pattern of PRY-1 in the later division – do DSH-2 and MIG-5 also have an unexpected localization pattern in the terminal seam cell division? Previously published fluorescent epitope-tagged DSH-2 and MIG-5 transgenes driven by the seam-cell-specific SCM promoter were used to visualize DSH-2 and MIG-5 localization in the later seam cell divisions (Mizumoto and Sawa, 2007). Both of these constructs had been reported to localize to the posterior cortex of the T seam cell that divides during the first larval phase (Mizumoto and Sawa, 2007).

We crossed *osEx233*(P_{scm}::MIG-5::YFP) with *uiwIs4* to observe MIG-5 and SYS-1 colocalization. At the very low levels of the *osEx233* extrachromosomal array expression, cortical asymmetry as previously recorded was observable (Fig. 5A). When MIG-5::VNS levels were low, SYS-1 asymmetry in the wild-type pattern was observed (Fig. 5A,D). At moderate levels of MIG-5::YFP expression, MIG-5 localized to the cytoplasm but was excluded from the nucleus (Fig. 5B). At this moderate level of MIG-5::YFP expression, SYS-1 levels and asymmetry remained unperturbed (Fig. 5B,D). Interestingly, at high to very high levels of MIG-5::YFP expression, cytoplasmic MIG-5 puncta began to form (Fig. 5C). These puncta were observable in mother cells prior to division and did not appear biased to either pole of the cell (Fig. S4A). With the appearance of MIG-5 puncta in these animals, SYS-1 puncta that colocalized with the MIG-5 puncta also became apparent (Fig. 5C). When SYS-1 nuclear levels were quantified in divisions where MIG-5 puncta were observed, anterior nuclear SYS-1 levels were significantly increased, resulting in SYS-1 nuclear symmetry (Fig. 5C,D). Puncta expressing both MIG-5 and SYS-1 were not observed to localize to the seam cell nuclei, and an increase in SYS-1 levels was not observed in the posterior nuclei, so the increase in anterior nuclear SYS-1 is not an artifact of quantification of punctate SYS-1. Thus, high levels of MIG-5 overexpression result in formation of MIG-5 puncta that then result in SYS-1 stabilization and symmetry.

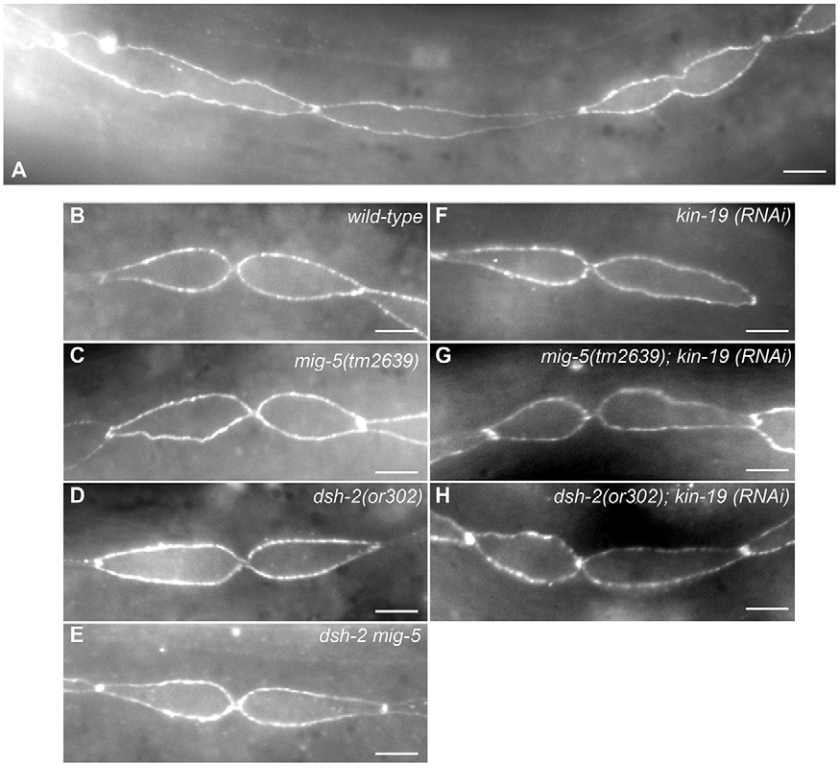

Fig. 4. PRY-1 cortical localization is symmetric at the terminal seam cell division. (A–G) Representative images of *osEx229*(P_{pry-1}::PRY-1::GFP) in seam cell daughter pairs. A, three adjacent wild-type seam cells, cell cycle stage from left to right: metaphase, anaphase, telophase; B, wild type; C, *mig-5(tm2639)*; D, *dsh-2(or302)*; E, *dsh-2(or302) mig-5(tm2639)*; F, *kin-19(RNAi)*; G, *mig-5 (tm2639); kin-19(RNAi)*; H, *dsh-2(or302); kin-19(RNAi)*. Scale bars: 5 µm.

Journal of Cell Science (2016) 129, 983-993 doi:10.1242/jcs.175802

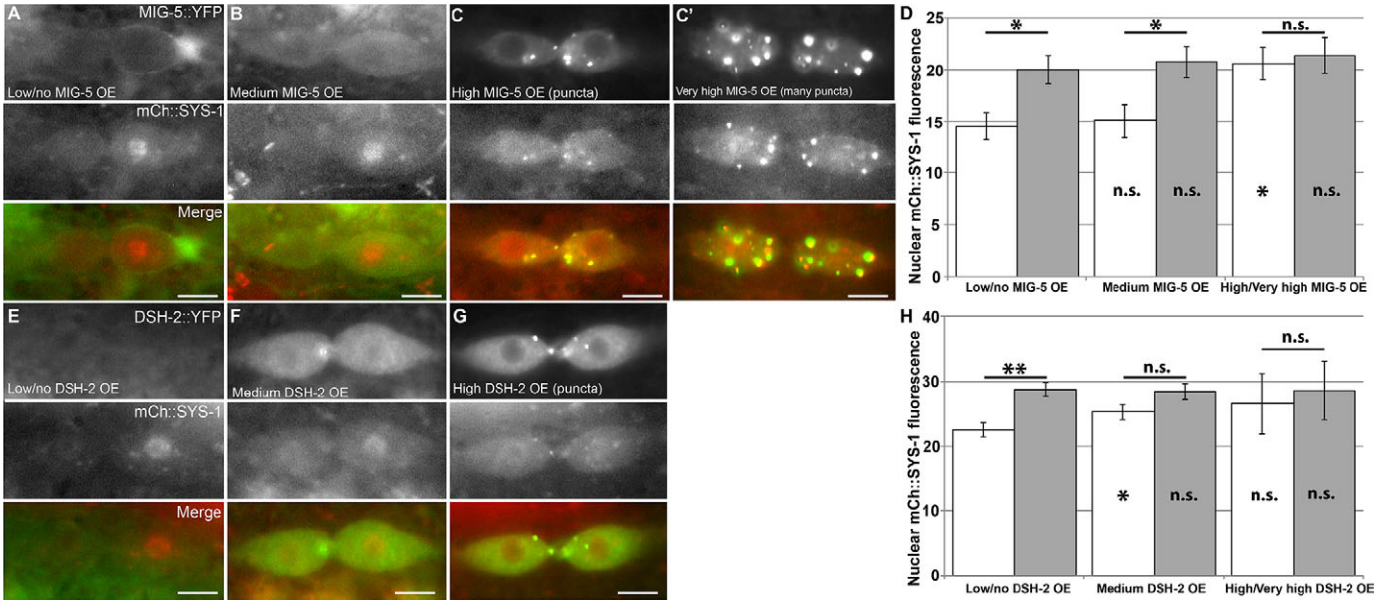

Fig. 5. MIG-5 and DSH-2 overexpression result in SYS-1 stabilization. (A–C′) Top rows, *osEx233*(P_{scm}::MIG-5::YFP);middle rows, *uiwIs4*(P_{sys-1}::mCherry::SYS-1); bottom rows, merge. (A) A representative image of low to unobservable levels of MIG-5::YFP overexpression (OE). (B) A representative image of medium levels of MIG-5::YFP overexpression. (C) A representative image of high to very high levels of MIG-5::YFP overexpression, with few (C) and many (C′) MIG-5::YFP puncta, respectively. (D) Mean±s.e.m. mCherry::SYS-1 nuclear intensity. *n*=20 (low or no MIG-5 overexpression), 11 (medium MIG-5 overexpression), 14 (high or very high MIG-5 overexpression). (E–G) Top rows, *osEx225*(P_{scm}::DSH-2::YFP); middle rows, *uiwIs4*(P_{sys-1}::mCherry::SYS-1); bottom rows, merge. (E) A representative image of low to unobservable levels of DSH-2::YFP overexpression (OE). (F) A representative image of medium levels of DSH-2::YFP overexpression. (G) A representative image of high levels of DSH-2::YFP overexpression with few DSH-2::YFP puncta. (H) Mean±s.e.m. mCherry::SYS-1 nuclear intensity. *n*=46 (low or no DSH-2 overexpression), 36 (medium DSH-2 overexpression), 6 (high DSH-2 overexpression). White columns in D and H indicate anterior nucleus fluorescence; gray columns indicate posterior nucleus fluorescence. Asterisks inside columns indicate statistical comparison to corresponding wild-type column. Horizontal lines represent the statistical comparisons indicated. **P*<0.05; ***P*<0.01; n.s., *P*>0.05 (Mann–Whitney test). Scale bars: 5 µm.

We also combined *osEx225* (P_{scm}::DSH-2::YFP) with *uiwIs4* to observe DSH-2 and SYS-1 colocalization. Similar to with MIG-5::YFP, DSH-2::YFP could be observed to be excluded from the nucleus, and DSH-2::YFP puncta would form in some cells that were observable before and after division (Fig. 5F,G, Fig. S4B). In contrast to MIG-5, clear asymmetric cortical localization of DSH-2::YFP was never observed, and although DSH-2::YFP puncta colocalized with mCherry::SYS-1, their overlap was less frequent (Fig. 5E,G; Fig. S4). DSH-2-overexpressing cell pairs were categorized into three classes: low to non-observable, medium, and high or displaying puncta (Fig. 5E–H). SYS-1 levels in daughter pairs with low to no DSH-2::YFP overexpression showed the wild-type pattern of nuclear SYS-1 asymmetry (Fig. 5E,H). However, in cells with medium levels of DSH-2::YFP overexpression, the average SYS-1 nuclear intensity in the anterior daughters was significantly higher than in cells with low or no DSH-2::YFP overexpression (Fig. 5F,H). Conversely, average SYS-1 nuclear intensity in cells with high levels of DSH-2::YFP overexpression (or displaying puncta) was not statistically different from cells with low or no DSH-2::YFP overexpression; we believe this is due to the rarity of this phenotype, leading to our low N-value and statistical power (Fig. 5G,H). From these data, we conclude that DSH-2 overexpression results in SYS-1 stabilization in anterior seam cell daughters.

DISCUSSION

Here, we provide insight into how cellular signals are transduced upon Wnt activation by uncovering the roles of the Dvl homologs DSH-2 and MIG-5 in regulating downstream effectors of WβA signaling in the seam cells of *C. elegans*. Mutation of each Dvl individually results in observable alterations in seam cell number, whereas loss of both Dvls results in increased seam cell fate specification defects compared to either single mutant. Furthermore, DSH-2 and MIG-5 positively regulate SYS-1 nuclear levels, as *dsh-2* and *mig-5* single mutants as well as the *dsh-2 mig-5* double mutant have lower SYS-1 levels compared to wild type. We also show that loss of MIG-5 results in loss of nuclear WRM-1 polarity through a reduction of posterior nuclear levels of WRM-1, whereas loss of DSH-2 appears to have a milder WRM-1 polarity defect. Loss of both MIG-5 and DSH-2 results in an increase in the average amount of nuclear WRM-1 in both anterior and posterior nuclei, indicating that together DSH-2 and MIG-5 negatively regulate nuclear WRM-1 levels. In the final seam cell division, we show that PRY-1 localizes symmetrically to the cortex of seam cell daughters, and that mutation of *dsh-2* and/or *mig-5* does not alter localization of PRY-1. Finally, overexpression of either MIG-5 or DSH-2 in the seam cells results in SYS-1 stabilization in the anterior (i.e. unsignaled) daughter. Overall, DSH-2 and MIG-5 fit a scheme of Wnt/β-catenin signaling specialized for ACD that is continuing to grow in complexity but offers both interesting similarities and departures from the canonical models of Wnt/β-catenin signaling, as depicted in Fig. 6 and discussed below.

Dvl is required for cell fate specification

Our initial finding was that DSH-2 and MIG-5 redundantly control seam cell fate, although the defects in seam cell fate specification were mild in either mutant. For example, up to 22 seam cells were observed in *mig-5* mutants versus the average of 16 in wild type, a gain of six seam cells (Fig. 1). Such a gain suggests that only six out of the 40 or more asymmetric seam cell divisions that occur from L1

Journal of Cell Science (2016) 129, 983-993 doi:10.1242/jcs.175802

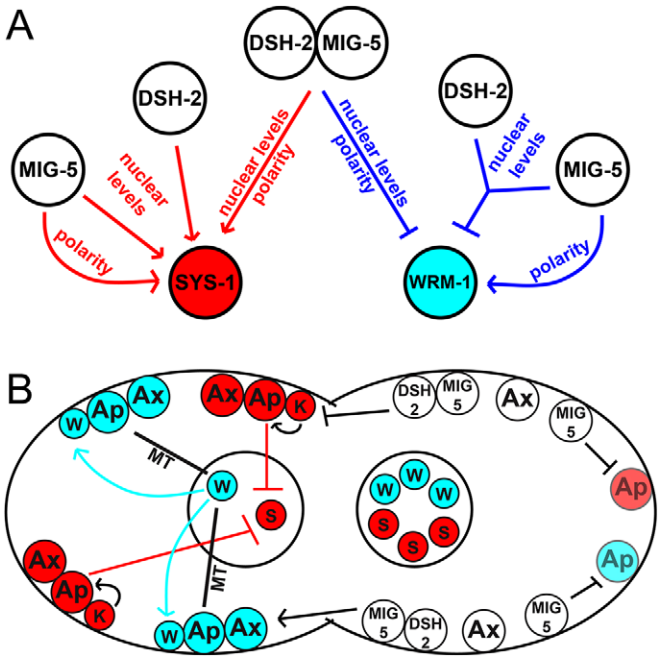

Fig. 6. Summary of data and model of differential control of the β-catenins WRM-1 and SYS-1 by MIG-5 and DSH-2. (A) Summary of DSH-2 and MIG-5 control of β-catenin localization during asymmetric seam cell division. Together, DSH-2 and MIG-5 positively regulate SYS-1 levels and negatively regulate WRM-1 levels, while controlling polarity of asymmetry of both β-catenins. The SYS-1-regulatory path is marked in red, and the WRM-1-regulatory path is marked in blue. In the case of WRM-1 regulation, DSH-2 and MIG-5 appear to redundantly and negatively regulate WRM-1 levels, but polarity of WRM-1 asymmetry appears to be controlled by MIG-5. Conversely, DSH-2 and MIG-5 are non-redundantly required to positively regulate SYS-1 levels, with MIG-5 again having a larger role in controlling polarity. (B) Model of Dvl function in WβA signaling pathway. DSH-2 and MIG-5 are likely controlling SYS-1 and WRM-1 nuclear levels by controlling the activity of APR-1 in the anterior daughter. MIG-5 controls polarity of APR-1, WRM-1 and SYS-1 localization by inhibiting posterior cortical localization of APR-1. PRY-1 localizes to the posterior cortex but its function there is unclear. S, SYS-1/β-catenin (red); W, WRM-1 (blue); Ax in red, SYS-1-regulating PRY-1; Ax in blue, WRM-1-regulating PRY-1; Ap in red, SYS-1-regulating APR-1; Ap in blue, WRM-1-regulating APR-1; K in red, KIN-19; MT, microtubules.

onward and are likely controlled by WβA had defective symmetric divisions in *mig-5* mutants. However, we also observed *dsh-2* and *mig-5* mutant worms with fewer than 16 seam cells, indicating that mutation of either protein can result in losses of seam cells as well as gains. Therefore, it is not accurate to simply label DSH-2 and MIG-5 as positive or negative regulators of seam cell fate; we provide possible hypotheses to explain these unusual phenotypes below.

One explanation for the mild seam cell fate phenotype is that gains and losses of seam cells through symmetric division mask each other in a final count of a large population of mutants. We observe gaps in the seam and clusters of extra seam cells in the same animals (Fig. 1C) suggesting that masking occurs within a single animal, likely causing our average seam cell counts to be an underestimation of the number of disrupted cell fate decisions. Gaps and clusters between seam cells were observed simultaneously in ~20% of Dvl mutant worms (data not shown), indicating that the phenotype of at least 20% of observed individual Dvl mutant animals would be underestimated by counting seam cells. Additionally, ~60% of Dvl mutants showed either gaps or clusters, suggesting that the phenotype of the overall mutant population is likely to be underrepresented by analyzing the average seam cell number. Although this explanation accounts for gains and losses of Dvl mutant seam cells as a population, individual seam cell defects can be explained by perturbations in downstream WβA regulators. We propose that the mild cell fate phenotype in *dsh-2* and *mig-5* mutants is due to the interaction between the SYS-1 and POP-1 branches, making WβA signaling robust to perturbation at the level of Dvl. For instance, the decrease in posterior WRM-1 nuclear levels in *mig-5* mutants would be predicted to increase nuclear POP-1 levels, which would then be predicted to repress WβA target genes in the seam cells and reduce seam cell number similar to in a *wrm-1* loss-of function (Banerjee et al., 2010; Gleason and Eisenmann, 2010; Ren and Zhang, 2010). The corresponding decrease in SYS-1 nuclear levels observed in *mig-5* mutants would be predicted to reduce seam cell numbers even further. However, we also observe that WRM-1 can be increased in the double mutant, which would result in increased seam cell number by moderately lowering nuclear POP-1, as in *pop-1(RNAi)* (Banerjee et al., 2010; Gleason and Eisenmann, 2010). Hence, the loss of Dvl has uncoupled reciprocal SYS-1 and POP-1 regulation, resulting in a confused seam cell fate that can occasionally cause symmetrical division. This uncoupled regulation of SYS-1 and POP-1 might then result in stochastic target gene expression and in the observed random gains and losses of seam cells in *mig-5* and *dsh-2* single mutants, as well as the moderate disruptions to seam cell number in the *dsh-2 mig-5* double mutant.

Alternatively, the mild Dvl loss-of-function phenotype could be due to upstream redundancy controlling WβA outputs. *The dsh-2* and *mig*-5 mutant cell fate phenotypes were surprising given that loss of downstream WβA components, such as *wrm-1*, *apr-1*, *kin-19* or *pop-1*, results in a much more severe seam cell fate defect (Banerjee et al., 2010; Gleason and Eisenmann, 2010; Ren and Zhang, 2010). Thus, the seam cells remain more biased towards asymmetric division in the absence of DSH-2 or MIG-5 than in the absence of more downstream components. Interestingly, simultaneous mutation or knockdown of all known Wnt ligands or receptors in *C. elegans* still allows for some properly polarized seam cell divisions to occur, indicating that WβA signaling is also robust to disruptions upstream of DSH-2 and MIG-5 (Yamamoto et al., 2011). The reason for this robustness is currently unclear, but it might be the result of multiple signaling pathways converging on cell fate in the seam cells, just as WβA and Src signaling converge on cell fate in the early embryonic EMS cell division (Bei et al., 2002). Cell contacts among seam cells have been previously demonstrated to control asymmetric division of the seam cells, and such a mechanism might be redundantly controlling seam cell fate specification alongside Wnt, Fz and Dvl, but ultimately converging upon downstream WβA regulators such as SYS-1, WRM-1 and POP-1 (Austin and Kenyon, 1994).

Dvl proteins differentially control β-catenin asymmetry

Mutation of either *dsh-2* or *mig-5* individually results in a significant reduction in nuclear SYS-1 levels in both anterior and posterior nuclei, and mutation of both *dsh-2* and *mig-5* simultaneously results in further reduction of SYS-1 levels in the posterior daughter compared to *dsh-2* but not *mig-5* mutants (Fig. 2). Still, the *dsh-2 mig-5* double mutants exhibit a largely similar SYS-1 decrease phenotype to the *dsh-2* and *mig-5* single mutants (Fig. 2), so then why and how are both Dvls required for WβA signaling? One answer is that WβA signaling combines not only both the β-catenin stabilization function of canonical Wnt/β-catenin signaling but also polarization of cortical proteins, both of

Journal of Cell Science (2016) 129, 983-993 doi:10.1242/jcs.175802

which are conserved functions of Dvl in both canonical and non-canonical Wnt pathways (Gao and Chen, 2010). Hence, a non-overlapping function of the two Dvls is revealed when comparing *mig-5* mutants to *dsh-2* mutants: loss of *mig-5* but not *dsh-2* abrogates SYS-1 asymmetry between the anterior and posterior nuclei, and similarly mutation of *mig-5* but not *dsh-2* results in significant disruption of cortical APR-1 localization. Thus, both DSH-2 and MIG-5 are capable of and necessary for the conserved β-catenin stabilization, but it appears that MIG-5 is responsible for the polarization of β-catenin stabilization (Fig. 6A). An alternative hypothesis that fits our data is that DSH-2 acts upstream of MIG-5 in SYS-1 regulation, posing the interesting problem of how multiple Dvls can act at different steps of an ordered genetic pathway. How these differences in function between DSH-2 and MIG-5 are effected by WβA signaling remains a mystery because DSH-2 and MIG-5 both contain the major conserved Dvl domains (PDZ, DEP and DIX), suggesting that difference in how DSH-2 and MIG-5 regulate and are regulated by WβA are dependent on more subtle differences in sequence and structure (Dillman et al., 2013).

dsh-2 mig-5 dual loss of function has been previously shown to result in loss of global POP-1 asymmetry in the POP-1-dependent asymmetric cell divisions in the early embryo (King et al., 2009). This finding is consistent with our discovery that the *dsh-2 mig-5* double mutant results in increased nuclear WRM-1 (Fig. 3), which is expected to result in symmetrically low nuclear POP-1. In contrast with the role of DSH-2 and MIG-5 in positive regulation of SYS-1, DSH-2 and MIG-5 redundantly function in negative regulation of WRM-1 nuclear localization (Fig. 3). What remains unclear is the degree of redundancy between DSH-2 and MIG-5 in polarizing WRM-1 nuclear localization. Our statistics fail to show a significant difference between anterior and posterior WRM-1 nuclear localization in both *dsh-2* and *mig-5*, but despite this *dsh-2* does not show a significant posterior reduction in nuclear WRM-1 compared to wild type (Fig. 3E). *mig-5* mutants, by contrast, do show a significant WRM-1 reduction. One explanation is that DSH-2 redundantly regulates WRM-1 nuclear levels alongside MIG-5, but that MIG-5 is primarily responsible for polarizing WRM-1 asymmetry (Fig. 6A). This is a notable difference from regulation of SYS-1 levels as described above, where DSH-2 and MIG-5 appear to act non-redundantly.

Dvl regulation of the β-catenin destruction complex

Previously, we have shown that APR-1 is necessary for negative regulation of both SYS-1 and WRM-1 nuclear levels in the seam cells but PRY-1 is not required for SYS-1 negative regulation. Instead PRY-1 is required for proper polarization of APR, which is then read out as SYS-1 and WRM-1 asymmetry (Baldwin and Phillips, 2014). Furthermore, we have shown that the SYS-1- and WRM-1-regulatory roles of APR-1 are genetically separable, and we hypothesized that Wnt signaling separates APR-1 into distinct functional pools for SYS-1 and WRM-1 regulation (Baldwin and Phillips, 2014). Building on our prior model, we show that MIG-5 controls APR-1 cortical localization and that both DSH-2 and MIG-5 are involved in regulation of SYS-1 and WRM-1 (Figs 2 and 3). Given that *dsh-2* and *mig-5* mutants do not disrupt PRY-1 localization (Fig. 4), it is likely that DSH-2 and MIG-5 are controlling SYS-1 and WRM-1 localization through APR-1 (Fig. 6B). Furthermore, because the *dsh-2 mig-5* double mutant results in increased nuclear WRM-1 but decreased nuclear SYS-1, it is likely that DSH-2 and MIG-5 are involved in the separation of APR-1 into its SYS-1- and WRM-1-regulatory pools. Specifically, it appears that DSH-2 and MIG-5 together activate the WRM-1-regulatory pool of APR-1 and inhibit the SYS-1-regulatory pool of APR-1. Given that the phenotype of *kin-19* RNAi closely resembles the phenotype of *mig-5* for SYS-1, WRM-1 and APR-1 localization (Baldwin and Phillips, 2014), MIG-5 likely cooperates with KIN-19 to regulate APR-1, potentially phosphorylating APR-1 to change its localization and/or activity.

That PRY-1 appears to localize symmetrically to seam cell cortices during their final division was also a surprising finding (Fig. 4). An earlier report that describes asymmetric PRY-1 cortical localization analyzed the earlier V5.p seam cell division, whereas our experiments examined the later, final seam cell division (Mizumoto and Sawa, 2007). Interestingly, this earlier paper reported that PRY-1 had no function in WRM-1 regulation; our previous work reported that PRY-1 does control the WRM-1 in the later seam cell division, indicating that there might be a profound difference in PRY-1-mediated regulation and function between the V5.p division and the terminal division (Baldwin and Phillips, 2014; Mizumoto and Sawa, 2007). Why these differences in WβA function exist within the seam cells at different times during development is unclear, but it has been hypothesized that differences in seam cell size between earlier and later divisions might account for differences in function of WβA components between earlier and later seam cell divisions (Kanamori et al., 2008). The observation of symmetric cortical localization of PRY-1 calls into question how PRY-1 controls an asymmetric process. We propose that a physical interaction between MIG-5 and PRY-1 on the posterior cortex prevents a PRY-1–APR-1 interaction in the posterior daughter, restricting cortical APR-1 to the anterior daughter. Interestingly, yeast two-hybrid experiments have previously shown that MIG-5 physically interacts with PRY-1; hence, the fact that mutation of either *mig-5* or *pry-1* results in polarity defects in both APR-1 and WRM-1 localization indicates that the MIG-5–PRY-1 interaction might be important for polarizing cortical APR-1 (Baldwin and Phillips, 2014; Korswagen et al., 2002). Consistent with the hypothesis that MIG-5 is more important than DSH-2 for mediating an APR-1–PRY-1 interaction, the previous yeast two-hybrid experiment failed to show an interaction between PRY-1 and DSH-2 (Korswagen et al., 2002). The biological relevance of a negative yeast two-hybrid result is debatable, but if this reflects how MIG-5 and DSH-2 interact with PRY-1 within a seam cell, it potentially explains how MIG-5 bears the brunt of polarizing APR-1 activity whereas DSH-2 does not.

Conserved Dvl function in asymmetric cell division

Our Dvl overexpression experiments provided both expected and unexpected results. That overexpression of Dvl results in stabilization of β-catenin is not so surprising in light of the commonly accepted positive role of Dvl proteins in Wnt signaling and our finding that *C. elegans* Dvl stabilize SYS-1, but the way by which each Dvl protein accomplished this was intriguing. Significant SYS-1 enrichment was observed in cells overexpressing both MIG-5 and DSH-2, but this increase in SYS-1 was correlated with MIG-5 and not DSH-2 puncta formation (Fig. 5). Given the intense interest in Fz- and Dvl-mediated regulation of the destruction complex, the nature and composition of the MIG-5 puncta is an interesting question for future investigation. Whether they are simply MIG-5 aggregates or perhaps the destruction-complex-containing ‘signalosomes’ described in other reports on Wnt signaling (Bilić et al., 2007; Taelman et al., 2010), the ability of these MIG-5 complexes to stabilize and colocalize with β-catenin is

Journal of Cell Science (2016) 129, 983-993 doi:10.1242/jcs.175802

clear. Conversely, DSH-2 overexpression was able to achieve modest β-catenin stabilization without the formation of visible puncta. Whether this represents a legitimate biological difference in the mode of action between MIG-5 and DSH-2 remains to be seen.

The precise role of Dvl in the canonical Wnt/β-catenin signaling cascade remains puzzling mainly because the precise mechanism of β-catenin destruction complex inactivation continues to evade us. In most systems of canonical Wnt/β-catenin signaling, the action of Dvl is presumed to be to sequester and inactivate Axin. Here, we have shown that Dvl loss of function does not alter Axin localization in a live cell that is responding to Wnt signaling. In addition, we show that Dvl proteins are controlling β-catenin localization independently of Axin localization, likely through APC and perhaps dependent on the regulatory state of Axin, rather than the quantity of cortical Axin. Given that vertebrates also possess multiple Dvl proteins that have been shown to have redundant roles in various gross developmental processes, the genetic interactions of MIG-5 and DSH-2 may inform how Dvls cooperate in vertebrate Wnt signaling (Etheridge et al., 2008). We demonstrate how multiple Dvl homologs within a single cell/system could have individualized roles in Wnt signaling despite having a singular function, i.e. control of β-catenin nuclear levels. Dvl has been called 'the hub of Wnt signaling', as it is the signaling protein that appears to truly unifies the 'Wnt' pathways (Gao and Chen, 2010). Our data presented here describes the complex mechanisms by which Dvls can manage the multiple potential outputs of Wnt signaling in a single cell, better elucidating the function of a class of proteins whose role in Wnt signaling is paradoxically well-known but little understood.

MATERIALS AND METHODS

Strains

Strains used in this study were: BTP105 [uiwIs4 (P_{sys-1}::mCherry::SYS-1)]; BTP118 [unc-76V; osIs13 (P_{apr-1}::APR-1::VNS; unc-76 (+)), uiwIs4]; HS1325 [unc-76(e911) V; osEx229 (P_{pry-1}::PRY-1::GFP+unc-76(+))]; HS1417 [osIs5 (P_{scm}::WRM-1::YFP) II]; JR 667 [unc-119(e2498::Tc1) III; wIs51(P_{scm}::GFP) V]; BTP137 [dsh-2(or302)/mIn1(dpy-10(e128), mIs14) II; osIs13, uiwIs4]; BTP138 [mig-5(tm2639)/mIn1(dpy-10(e128), mIs14) II; osIs13, uiwIs4]; BTP139 [dsh-2(or302) mig-5(tm2639)/mIn1(dpy-10(e128), mIs14) II; osIs13, uiwIs4]; BTP143 [mig-5(tm2639)/mIn1(dpy-10(e128), mIs14) II; ws51V]; BTP144 [dsh-2(or302)/mIn1(dpy-10(e128), mIs14) II; wIs51V]; BTP145 [dsh-2(or302) mig-5(tm2639)/mIn1(dpy-10(e128), mIs14) II; wIs51V]; BTP148 [dsh-2(or302)/mIn1(dpy-10(e128), mIs14) II; unc-76(e911) V; osEx229]; BTP182 [unc-76(e911) V; uiwIs4; osEx233 (P_{scm}::MIG-5::YFP+unc-76(+))]; BTP183 [unc-76(e911) V; osEx225 (P_{scm}::DSH-2::YFP+unc-76(+))]; BTP185 [dsh-2(or302) mig-5(tm2639)/mIn1(dpy-10(e128), mIs14) II; uiwIs4]; BTP161 [dsh-2(or302),osIs5/mIn1(dpy-10(e128), mIs14) II]; BTP167 [mig-5(tm2639),osIs5/mIn1(dpy-10(e128), mIs14) II]; BTP175 [mig-5(tm2639)/mIn1[dpy-10(e128), mIs14] II;unc-76(e911) V; osEx229]; BTP184 [dsh-2(or302) mig-5(tm2639),osIs5/mIn1(dpy-10(e128), mIs14) II]; BTP194 [mig-5(tm2639)/mIn1(dpy-10(e128), mIs14) II; uiwIs4]; BTP195 [dsh-2(or302) mig-5(tm2639)/mIn1(dpy-10(e128), mIs14) II; uiwIs4]; BTP197 [dsh-2(or302) mig-5(tm2639)/mIn1(dpy-10(e128), mIs14) II; unc-76(e911) V; osEx229]; BTP200 [dsh-1(ok1445), wIs51V].

Larvae analysis

RNAi was performed using standard techniques using the pL4440 feeding vector (Timmons et al., 2001). Synchronized L1 worms were grown at 20°C until late L3 when the terminal seam cell division occurs. L3 worms were then immobilized using 10 µM muscimol on 6% agarose pads for live imaging. Cells and their corresponding nuclei were identified through differential interference contrast (DIC) microscopy prior to fluorescence image capture; *n* values refer to the number of daughter pairs imaged and compared. Box plots in Fig. 1 were assembled using the Tyers Lab tool (Spitzer et al., 2014).

Fluorescence quantification

Images were obtained using Zeiss Axio Imager.D2 compound fluorescent scope and Zeiss Zen software. Raw image data was exported into TIFF format and analyzed using ImageJ software. Nuclei of seam cells were identified in DIC images and then the mean protein fluorescence in fluorescent images was quantified using ImageJ. Background fluorescence was normalized for each experiment by using the same channels and exposures to image seam cells in N2 wild-type worms (n=24 for each exposure setting). All statistical comparisons were performed with either a *t*-test in Microsoft Excel or the Mann–Whitney test and VassarStats software (VassarStats, Lowry, 2010).

Acknowledgements

We would like to thank Doug Houston, Jan Fassler, Lori Adams, and the Phillips laboratory for helpful comments during the development of the manuscript. Many strains and transgenes were provided by the Caenorhabditis Genetics Center, which is funded by the NIH Office of Research Infrastructure Programs [grant number P40 OD01440].

Competing interests

The authors declare no competing or financial interests.

Author contributions

A.T.B. designed and performed experiments and wrote the manuscript. A.M.C. performed experiments. B.T.P. designed experiments and wrote the manuscript.

Funding

The research performed in this paper was supported by the American Cancer Society and the Holden Comprehensive Cancer Center [grant numbers RSG-11-140-01-DC and IRG# 77-004-31 to B.T.P.]; the Roy J. Carver Charitable Trust [grant number 13-4131 to B.T.P.]; and the National Science Foundation [grant number IOS-1456941 to B.T.P.]; and an Evelyn Hart Watson fellowship to A.T.B.

Supplementary information

Supplementary information available online at
http://jcs.biologists.org/lookup/suppl/doi:10.1242/jcs.175802/-/DC1

References

Austin, J. and Kenyon, C. (1994). Cell contact regulates neuroblast formation in the Caenorhabditis elegans lateral epidermis. *Development* **120**, 313-323.

Baldwin, A. T. and Phillips, B. T. (2014). The tumor suppressor APC differentially regulates multiple β-catenins through the function of axin and CKIα during C. elegans asymmetric stem cell divisions. *J. Cell Sci.* **127**, 2771-2781.

Banerjee, D., Chen, X., Lin, S. Y. and Slack, F. J. (2010). kin-19/casein kinase Iα has dual functions in regulating asymmetric division and terminal differentiation in C. elegans epidermal stem cells. *Cell Cycle* **9**, 4748-4765.

Barker, N., Ridgway, R. A., van Es, J. H., van de Wetering, M., Begthel, H., van den Born, M., Danenberg, E., Clarke, A. R., Sansom, O. J. and Clevers, H. (2009). Crypt stem cells as the cells-of-origin of intestinal cancer. *Nature* **457**, 608-611.

Bei, Y., Hogan, J., Berkowitz, L. A., Soto, M., Rocheleau, C. E., Pang, K. M., Collins, J. and Mello, C. C. (2002). SRC-1 and Wnt signaling act together to specify endoderm and to control cleavage orientation in early C. elegans embryos. *Dev. Cell* **3**, 113-125.

Bilić, J., Huang, Y.-L., Davidson, G., Zimmermann, T., Cruciat, C.-M., Bienz, M. and Niehrs, C. (2007). Wnt induces LRP6 signalosomes and promotes dishevelled-dependent LRP6 phosphorylation. *Science* **316**, 1619-1622.

Chang, W., Lloyd, C. E. and Zarkower, D. (2005). DSH-2 regulates asymmetric cell division in the early C. elegans somatic gonad. *Mech. Dev.* **122**, 781-789.

Clevers, H. and Nusse, R. (2012). Wnt/β-catenin signaling and disease. *Cell* **149**, 1192-1205.

Cliffe, A., Hamada, F. and Bienz, M. (2003). A role of Dishevelled in relocating Axin to the plasma membrane during wingless signaling. *Curr. Biol.* **13**, 960-966.

Costa, M., Draper, B. W. and Priess, J. R. (1997). The role of actin filaments in patterning the Caenorhabditis elegans cuticle. *Dev. Biol.* **184**, 373-384.

Dillman, A. R., Minor, P. J. and Sternberg, P. W. (2013). Origin and evolution of dishevelled. *G3* **3**, 251-262.

Etheridge, S. L., Ray, S., Li, S., Hamblet, N. S., Lijam, N., Tsang, M., Greer, J., Kardos, N., Wang, J., Sussman, D. J. et al. (2008). Murine dishevelled 3 Functions in redundant pathways with dishevelled 1 and 2 in normal cardiac outflow tract, cochlea, and neural tube development. *PLoS Genet.* **4**, e1000259.

Fiedler, M., Mendoza-Topaz, C., Rutherford, T. J., Mieszczanek, J. and Bienz, M. (2011). Dishevelled interacts with the DIX domain polymerization interface of Axin to interfere with its function in down-regulating β-catenin. *Proc. Natl. Acad. Sci. USA* **108**, 1937-1942.

Gao, C. and Chen, Y.-G. (2010). Dishevelled: the hub of Wnt signaling. *Cell. Signal.* **22**, 717-727.
Gessert, S. and Kühl, M. (2010). The multiple phases and faces of wnt signaling during cardiac differentiation and development. *Circ. Res.* **107**, 186-199.
Gleason, J. E. and Eisenmann, D. M. (2010). Wnt signaling controls the stem cell-like asymmetric division of the epithelial seam cells during C. elegans larval development. *Dev. Biol.* **348**, 58-66.
Gorrepati, L., Thompson, K. W. and Eisenmann, D. M. (2013). C. elegans GATA factors EGL-18 and ELT-6 function downstream of Wnt signaling to maintain the progenitor fate during larval asymmetric divisions of the seam cells. *Development* **140**, 2093-2102.
Groden, J., Thliveris, A., Samowitz, W., Carlson, M., Gelbert, L., Albertsen, H., Joslyn, G., Stevens, J., Spirio, L., Robertson, M. et al. (1991). Identification and characterization of the familial adenomatous polyposis coli gene. *Cell* **66**, 589-600.
Hawkins, N. C., Ellis, G. C., Bowerman, B. and Garriga, G. (2005). MOM-5 frizzled regulates the distribution of DSH-2 to control C. elegans asymmetric neuroblast divisions. *Dev. Biol.* **284**, 246-259.
Hikasa, H. and Sokol, S. Y. (2013). Wnt signaling in vertebrate axis specification. *Cold Spring Harb. Perspect. Biol.* **5**, a007955.
Houston, D. W. (2012). Cortical rotation and messenger RNA localization in Xenopus axis formation. *Wiley Interdiscip. Rev. Dev. Biol.* **1**, 371-388.
Huang, S., Shetty, P., Robertson, S. M. and Lin, R. (2007). Binary cell fate specification during C. elegans embryogenesis driven by reiterated reciprocal asymmetry of TCF POP-1 and its coactivator beta-catenin SYS-1. *Development* **134**, 2685-2695.
Hughes, S., Brabin, C., Appleford, P. J. and Woollard, A. (2013). CEH-20/Pbx and UNC-62/Meis function upstream of rnt-1/Runx to regulate asymmetric divisions of the C. elegans stem-like seam cells. *Biol. Open.* **2**, 718-727.
Itoh, K., Antipova, A., Ratcliffe, M. J. and Sokol, S. (2000). Interaction of dishevelled and xenopus axin-related protein is required for Wnt signal transduction. *Mol. Cell. Biol.* **20**, 2228-2238.
Kanamori, T., Inoue, T., Sakamoto, T., Gengyo-Ando, K., Tsujimoto, M., Mitani, S., Sawa, H., Aoki, J. and Arai, H. (2008). Beta-catenin asymmetry is regulated by PLA1 and retrograde traffic in C. elegans stem cell divisions. *EMBO J.* **27**, 1647-1657.
Khramtsov, A. I., Khramtsova, G. F., Tretiakova, M., Huo, D., Olopade, O. I. and Goss, K. H. (2010). Wnt/beta-catenin pathway activation is enriched in basal-like breast cancers and predicts poor outcome. *Am. J. Pathol.* **176**, 2911-2920.
King, R. S., Maiden, S. L., Hawkins, N. C., Kidd, A. R., III, Kimble, J., Hardin, J. and Walston, T. D. (2009). The N- or C-terminal domains of DSH-2 can activate the C. elegans Wnt/beta-catenin asymmetry pathway. *Dev. Biol.* **328**, 234-244.
Korswagen, H. C., Coudreuse, D. Y. M., Betist, M. C., van de Water, S., Zivkovic, D. and Clevers, H. C. (2002). The Axin-like protein PRY-1 is a negative regulator of a canonical Wnt pathway in C. elegans. *Genes Dev.* **16**, 1291-1302.
Lee, E., Salic, A., Krüger, R., Heinrich, R. and Kirschner, M. W. (2003). The roles of APC and axin derived from experimental and theoretical analysis of the Wnt pathway. *PLoS Biol.* **2**, e89.
Li, V. S. W., Ng, S. S., Boersema, P. J., Low, T. Y., Karthaus, W. R., Gerlach, J. P., Mohammed, S., Heck, A. J. R., Maurice, M. M., Mahmoudi, T. et al. (2012). Wnt signaling through inhibition of β-catenin degradation in an intact axin1 complex. *Cell* **149**, 1245-1256.
Liu, Z., Kirch, S. and Ambros, V. (1995). The Caenorhabditis elegans heterochronic gene pathway controls stage-specific transcription of collagen genes. *Development* **121**, 2471-2478.
Mao, J., Wang, J., Liu, B., Pan, W., Farr, G. H., III, Flynn, C., Yuan, H., Takada, S., Kimelman, D., Li, L. et al. (2001). Low-density lipoprotein receptor-related protein-5 binds to Axin and regulates the canonical Wnt signaling pathway. *Mol. Cell* **7**, 801-809.
McMahon, A. P. and Moon, R. T. (1989). Ectopic expression of the proto-oncogene int-1 in Xenopus embryos leads to duplication of the embryonic axis. *Cell* **58**, 1075-1084.
Mizumoto, K. and Sawa, H. (2007). Cortical beta-catenin and APC regulate asymmetric nuclear beta-catenin localization during asymmetric cell division in C. elegans. *Dev. Cell* **12**, 287-299.
Phillips, B. T. and Kimble, J. (2009). A new look at TCF and beta-catenin through the lens of a divergent C. elegans Wnt pathway. *Dev. Cell* **17**, 27-34.
Phillips, B. T., Kidd, A. R., III, King, R., Hardin, J. and Kimble, J. (2007). Reciprocal asymmetry of SYS-1/beta-catenin and POP-1/TCF controls asymmetric divisions in Caenorhabditis elegans. *Proc. Natl. Acad. Sci. USA* **104**, 3231-3236.
Ren, H. and Zhang, H. (2010). Wnt signaling controls temporal identities of seam cells in Caenorhabditis elegans. *Dev. Biol.* **345**, 144-155.
Rocheleau, C. E., Yasuda, J., Shin, T. H., Lin, R., Sawa, H., Okano, H., Priess, J. R., Davis, R. J. and Mello, C. C. (1999). WRM-1 activates the LIT-1 protein kinase to transduce anterior/posterior polarity signals in C. elegans. *Cell* **97**, 717-726.
Roose, J., Molenaar, M., Peterson, J., Hurenkamp, J., Brantjes, H., Moerer, P., van de Wetering, M., Destrée, O. and Clevers, H. (1998). The Xenopus Wnt effector XTcf-3 interacts with Groucho-related transcriptional repressors. *Nature* **395**, 608-612.
Sawa, H. (2012). Control of cell polarity and asymmetric division in C. elegans. *Curr. Top. Dev. Biol.* **101**, 55-76.
Singh, R. N. and Sulston, J. E. (1978). Some observations on moulting in Caenorhabditis elegans. *Nematologica* **24**, 63-71.
Spitzer, M., Wildenhain, J., Rappsilber, J. and Tyers, M. (2014). BoxPlotR: a web tool for generation of box plots. *Nat. Methods* **11**, 121-122.
Sugioka, K. and Sawa, H. (2012). Formation and functions of asymmetric microtubule organization in polarized cells. *Curr. Opin. Cell Biol.* **24**, 517-525.
Sugioka, K., Mizumoto, K. and Sawa, H. (2011). Wnt regulates spindle asymmetry to generate asymmetric nuclear β-catenin in C. elegans. *Cell* **146**, 942-954.
Sulston, J. E. and Horvitz, H. R. (1977). Post-embryonic cell lineages of the nematode, Caenorhabditis elegans. *Dev. Biol.* **56**, 110-156.
Taelman, V. F., Dobrowolski, R., Plouhinec, J.-L., Fuentealba, L. C., Vorwald, P. P., Gumper, I., Sabatini, D. D. and De Robertis, E. M. (2010). Wnt signaling requires sequestration of glycogen synthase kinase 3 inside multivesicular endosomes. *Cell* **143**, 1136-1148.
Takeshita, H. and Sawa, H. (2005). Asymmetric cortical and nuclear localizations of WRM-1/beta-catenin during asymmetric cell division in C. elegans. *Genes Dev.* **19**, 1743-1748.
Thein, M. C., McCormack, G., Winter, A. D., Johnstone, I. L., Shoemaker, C. B. and Page, A. P. (2003). Caenorhabditis elegans exoskeleton collagen COL-19: an adult-specific marker for collagen modification and assembly, and the analysis of organismal morphology. *Dev. Dyn.* **226**, 523-539.
Timmons, L., Court, D. L. and Fire, A. (2001). Ingestion of bacterially expressed dsRNAs can produce specific and potent genetic interference in Caenorhabditis elegans. *Gene* **263**, 103-112.
Vora, S. and Phillips, B. T. (2015). Centrosome-associated degradation limits β-catenin inheritance by daughter cells after asymmetric division. *Curr. Biol.* **25**, 1005-1016.
Webster, M.-T., Rozycka, M., Sara, E., Davis, E., Smalley, M., Young, N., Dale, T. C. and Wooster, R. (2000). Sequence variants of the axin gene in breast, colon, and other cancers: an analysis of mutations that interfere with GSK3 binding. *Genes Chromosomes Cancer* **28**, 443-453.
Wildwater, M., Sander, N., de Vreede, G. and van den Heuvel, S. (2011). Cell shape and Wnt signaling redundantly control the division axis of C. elegans epithelial stem cells. *Development* **138**, 4375-4385.
Wong, H.-C., Bourdelas, A., Krauss, A., Lee, H.-J., Shao, Y., Wu, D., Mlodzik, M., Shi, D.-L. and Zheng, J. (2003). Direct binding of the PDZ domain of dishevelled to a conserved internal sequence in the C-terminal region of frizzled. *Mol. Cell* **12**, 1251-1260.
Yamamoto, Y., Takeshita, H. and Sawa, H. (2011). Multiple Wnts redundantly control polarity orientation in Caenorhabditis elegans epithelial stem cells. *PLoS Genet.* **7**, e1002308.

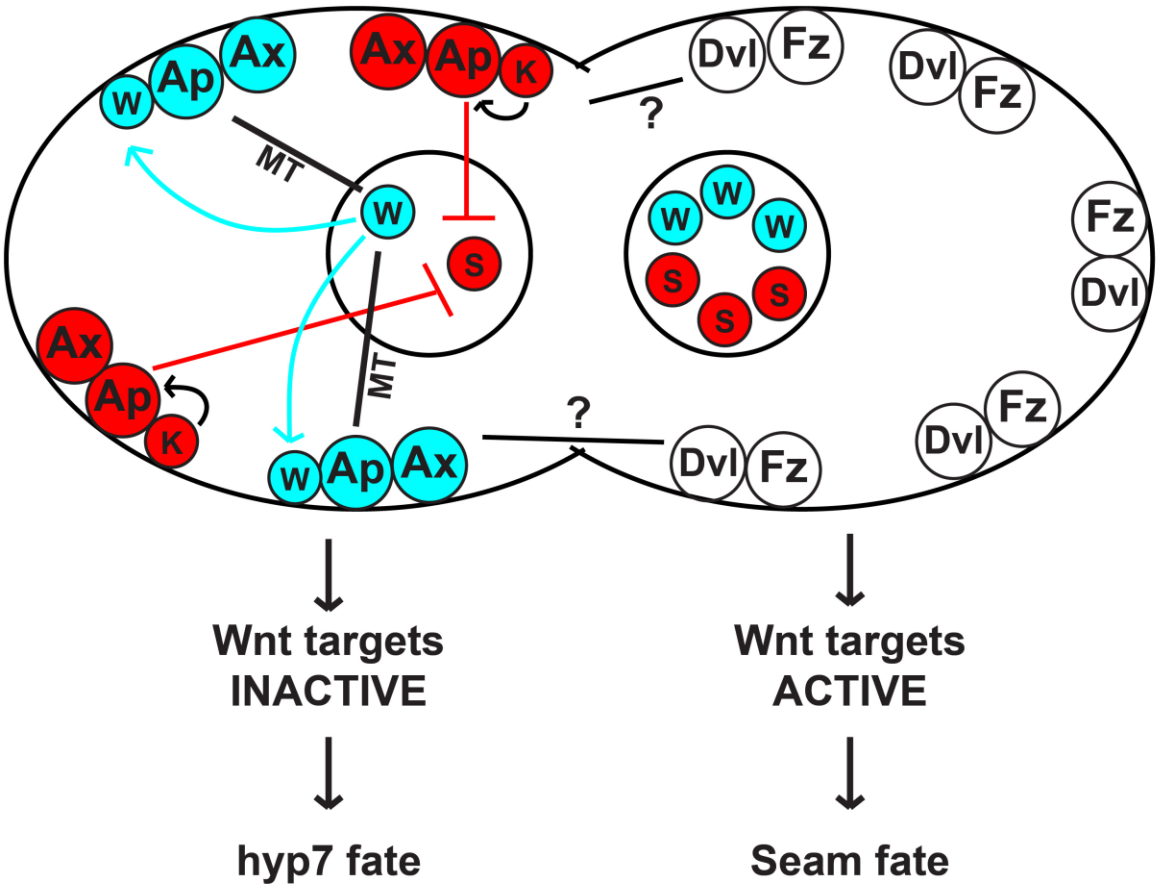

Figure S1: Model for β-catenin regulation in the seam cells of a wild type worm. Two pools of APR-1/APC are present in the anterior daughter, a microtubule-associated WRM-1-regulating pool (wrmAPR-1, shown in blue) and a KIN-19/CKIα associated SYS-1-regulating pool (sysAPR-1, shown in red). Polarized localization of both sysAPR-1 and wrmAPR-1 is controlled by PRY-1/Axin. Frizzled and Dishevelled presumably localize to the posterior daughter, but how they translate the polarity and activity signal to APR-1 is unknown (denoted by question marks). S, SYS-1/β-catenin (red); W, WRM-1/β-catenin (blue); Ax, SYS-1-regulating PRY-1/Axin (red) Ax, WRM-1-regulating PRY-1/Axin (blue); Ap, SYS-1-regulating APR-1/APC (red); Ap, WRM-1-regulating APR-1/APC (blue); K, KIN-19/CKIα (red); MT, microtubules; Fz, Frizzled; D, DSH-2, MIG-5/Dishevelled.

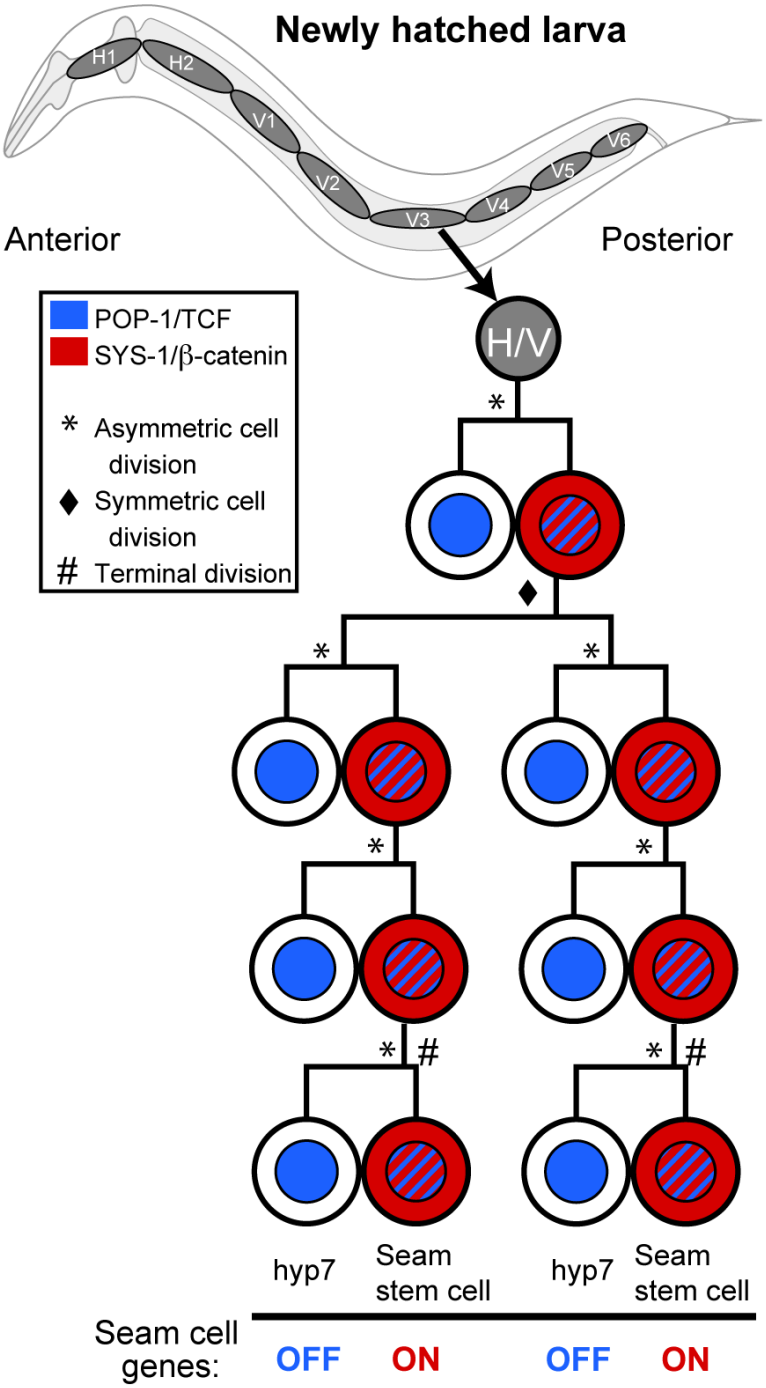

Figure S2: The epidermal seam cells divide in a stem cell-like pattern dependent on the WβA signaling pathway. A cartoon lineage of a representative seam cell. Nuclear POP-1/TCF is high in the anterior nuclei, resulting in target gene repression. Nuclear POP-1 is low in posterior in response to WRM-1/β-catenin-mediated nuclear export, SYS-1/β-catenin levels are high in response to stabilization, and Wnt targets are activated that result in adoption of the seam cell fate. Note that the "#" symbol marks the terminal/final seam cell division, upon which we focus our studies.

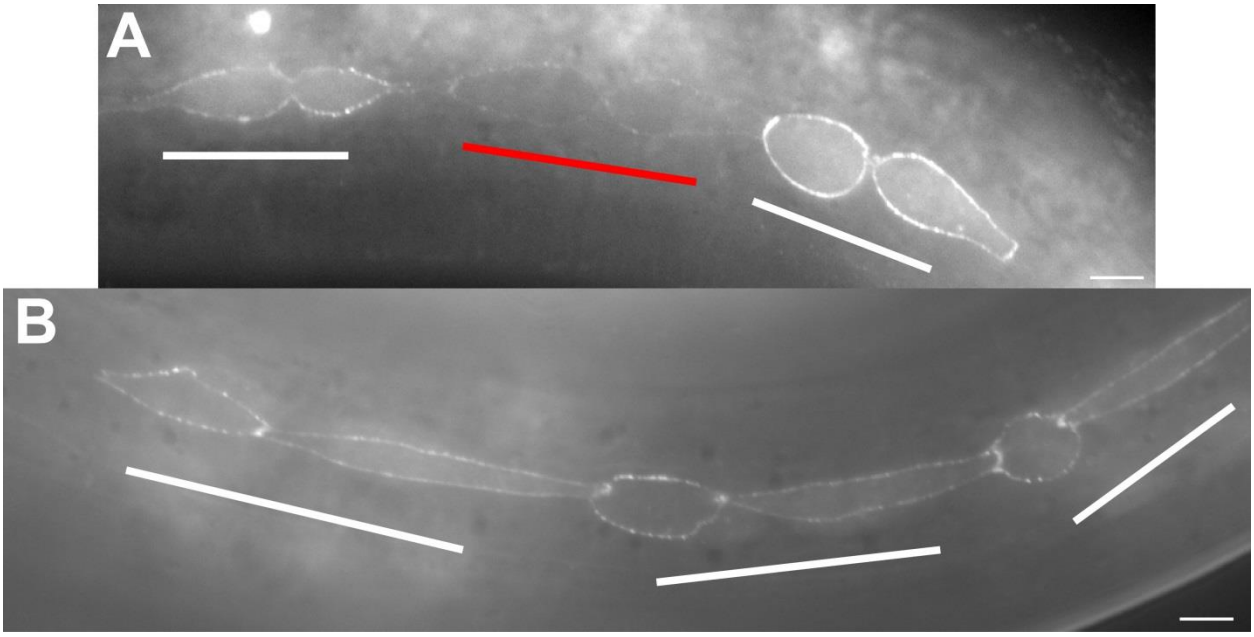

Figure S3: PRY-1::GFP localizes symmetrically to seam cell daughter cortices and does not alter cell fate specification. A, *osEx229(*$p_{pry\text{-}1}$::PRY-1::GFP) in wild-type seam cells. Lines indicate daughter pairs. The red line marks a daughter pair with lower *osEx229* expression that still displays symmetric PRY-1::GFP localization. B, *osEx229* expression after division and fate specification. White lines mark daughter pairs. The anterior daughters have correctly adopted the hyp7 fate and have become smaller and more rounded in anticipation of fusion with hyp7, while the posterior daughters have adopted the seam fate and begun elongation. Scale bars = 5 µm.

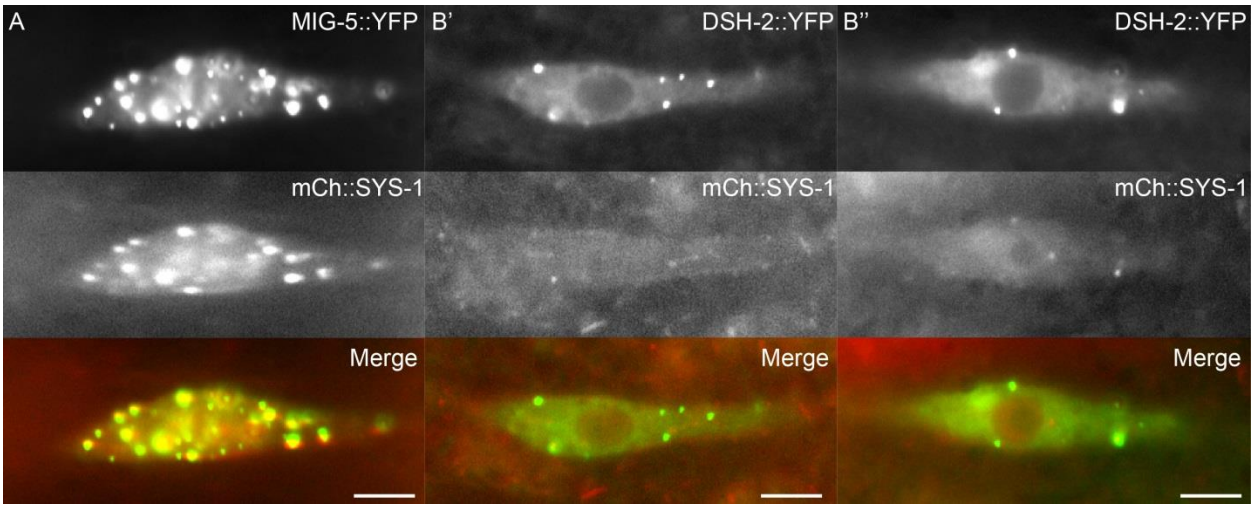

Figure S4: Dvl puncta are present prior to division. All images are representative of seam cell mothers in interphase that are expression high/punctate levels of Dvl overexpression. A, top panel: *osEx233*(p_{SCM}::MIG-5::YFP), middle panel: *uiwIs4*(p_{sys-1}::mCherry::SYS-1), bottom panel: merge. B' & B'', top panels: *osEx225*(p_{SCM}::DSH-2::YFP), middle panels: *uiwIs4*(p_{sys-1}::mCherry::SYS-1), bottom panels: merge. Scale bars = 5 µm.

Table S1: DSH-1 does not regulate seam cell fate. Seam cell counts were obtained in early adulthood using the *wIs51*(*scm*::GFP) reporter. EV = empty vector.

Genotype	RNAi treatment	Average seam cell number ± standard error	N-value
wild-type	EV	15.98 ± 0.07	62
wild-type	*dsh-1 RNAi*	15.96 ± 0.05	62
dsh-1(ok1445)	EV	16 ± 0.05	61
dsh-2(or302) mig-5(tm2639)	EV	17.66 ± 0.28	54
	dsh-1 RNAi	17.72 ± 0.27	59